Adaptive & Learning Control

DSC-Vol. 21

ADAPTIVE AND LEARNING CONTROL

PRESENTED AT
THE WINTER ANNUAL MEETING OF
THE AMERICAN SOCIETY OF MECHANICAL ENGINEERS
DALLAS, TEXAS
NOVEMBER 25–30, 1990

SPONSORED BY
THE DYNAMIC SYSTEMS AND CONTROL DIVISION, ASME

EDITED BY
NADER SADEGH
GEORGIA INSTITUTE OF TECHNOLOGY

THE AMERICAN SOCIETY OF MECHANICAL ENGINEERS
345 East 47th Street □□ United Engineering Center □□ New York, N.Y. 10017

ISBN No. 0-7918-0551-4

Library of Congress
Catalog Number 90-55906

FOREWORD

This volume contains papers presented in the Symposium on Adaptive and Learning Control held at the 1990 Winter Annual Meeting of The American Society of Mechanical Engineers (ASME). This symposium was held in Dallas, Texas on November 25-30, 1990. The symposium and the editing of this volume were sponsored by the Adaptive and Optimal Control Technical Panel of the Dynamic Systems and Control Division of the ASME.

The collection of papers that are presented here cover a wide spectrum of theoretical as well as application oriented issues of interest in the areas of adaptive, repetitive and learning control. The symposium is comprised of two technical sessions:

(1) Applied Adaptive Control, and
(2) Repetitive and Learning Control.

The papers in the first session cover subject matters such as adaptive control of two axis motion control systems, experimental investigation of adaptive and non-adaptive tracking controllers, gain scheduling technique, self tuning control of disk file servos, and time delay control systems. The subjects covered in the second session include learning control of robot manipulators, adaptive run-out correction system for disk drives, multivariable repetitive control, and intelligent control of systems with unknown dynamics.

I would like to thank all of the authors and the referees to whom much of the credit for success of this symposium is due. I would also like to thank Amy Tomasko of the Georgia Institute of Technology and Stacy Lambert of the University of Michigan for their invaluable secretarial assistance in putting all this together.

Nader Sadegh
Georgia Institute of Technology

CONTENTS

SYNCHRONIZATION OF TWO MOTION CONTROL AXES UNDER ADAPTIVE FEEDFORWARD CONTROL

Masayoshi Tomizuka, Jwu-Sheng Hu, and Tsu-Chih Chiu
Department of Mechanical Engineering
University of California
Berkeley, California

Takuya Kamano
Department of Electrical Engineering
The University of Tokushima
Tokushima, Japan

ABSTRACT

In this paper, motion synchronization of two DC motors, or motion control axes, under adaptive feedforward control is considered. The adaptive feedforward control system for each axis consists of a proportional feedback controller, an adaptive disturbance compensator and an adaptive feedforward controller. If the two adaptive systems are left uncoupled, a disturbance input applied to one of the two axes will cause a motion error in the disturbed axis only, and the error becomes the synchronization error. To achieve a better synchronization, a coupling controller, which responds to the synchronization error, i.e. the difference between the two motion errors, is introduced. In this case, when a disturbance input is applied to one axis, the motion errors appear in the undisturbed axis as well as in the disturbed axis. The motion error in the undisturbed axis is induced by the coupling controller and adaptive feedforward controller. The adaptive synchronizing problem is formulated and analyzed in the continuous time domain first, and then in the discrete time domain. Stability conditions are obtained. Effectiveness of the adaptive synchronizing controller is demonstrated by simulation.

INTRODUCTION

One fundamental problem in motion control systems is that a multiple number of motion axes or motors must be controlled in a synchronous manner. For example, in control of machine tools, a poor synchronization of relevant motion control axes results in diminished dimensional accuracy of the workpiece or even in unusable products. Synchronization can be achieved by either the "equal-status" approach or "master-slave" approach (Uchiyama and Nakamura, 1988). In the equal-status approach, the synchronizing controller treats multiple axes in a similar manner without favoring one axis over the other. When the dynamics are significantly different among multiple axes, the equal-status approach may not be the best because the synchronization speed of the overall system is set by the slowest axis. In a two-axes problem with significantly different dynamics between the two axes, it will make more sense to take the master-slave approach. In this case, the slow axis is under conventional servo control and acts as the master for the fast axis. The fast axis is the slave and follows the slow axis. In this paper, synchronization will be considered from the equal-status viewpoints. Other issues, which must be taken into consideration, are: 1. dynamics of motion axes may depend on operating conditions, and 2. motion axes must be synchronized during transient as well as at steady state. These issues are difficult to handle within a frame work of conventional feedback control theory. The objective of this paper is to explore the synchronization problem from the viewpoint of adaptive control: in particular, speed synchronization of two DC motors under adaptive feedforward control is considered.

In the next section, we first introduce an adaptive scheme for a one axis system, which consists of a proportional feedback controller, an adaptive disturbance compensator and an adaptive feedforward controller. For two axes systems, we introduce a coupling controller in addition to the adaptive feedforward controller for each axis. The coupling controller responds to the synchronization error, i.e. the difference between the two motion errors. This idea is similar to the one suggested by Koren (1980) for two axes contouring systems. The synchronization error is used as the adaptation error signal in the two adaptive feedforward controllers. The stability of this adaptive synchronizing system is analyzed. Simulation results will be shown to demonstrate the effectiveness of synchronizing control. In Section 3, we formulate the problem as a discrete time control problem and analyze its stability. Simulation will be repeated and compared with the continuous time case. Motivation for discrete time formulation is implementation by using a digital computer. Conclusions and future research directions will be described in Section 4.

ADAPTIVE SYNCHRONIZING CONTROL — CONTINUOUS TIME CASE

Adaptive Feedforward Control

Feedforward control is effective in tracking the time varying desired output signal (e.g. Tomizuka, 1989). However tracking performance under feedforward controllers depends on the accuracy of a plant model utilized in the design. When dynamic parameters such as viscous and Coulomb friction coefficients and inertia are subject to change, they must be estimated in real time and the feedforward controller must be adjusted accordingly. In this section, we consider an adaptive feedforward control approach and its use in a two-axes synchronizing problem. The adaptive feedforward control scheme is for regulation and

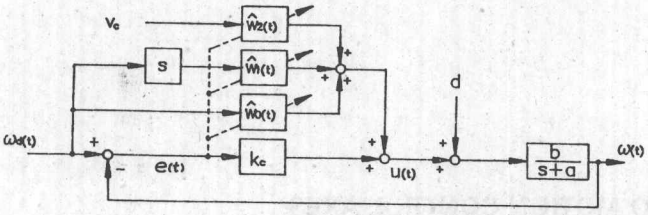

Fig. 1 Adaptive Feedforward Control System (Continuous Time)

tracking control of motor speed, and the overall system is as sketched in Fig. 1. The motor dynamics is described by

$$G(s) = b/(s + a), \quad a > 0 \text{ and } b > 0 \tag{1}$$

where the plant parameters a and b are not precisely known or subject to change. Typically, a and b depend on inertia load as well as viscous friction force. As shown in Fig. 1, the input to the motor is

$$u(t) = k_c e(t) + u_f(t) \tag{2}$$

where k_c is a fixed proportional control gain. $u_f(t)$ is the feedforward control input defined by

$$u_f(t) = \hat{w}_0(t)\omega_d(t) + \hat{w}_1(t)\{d\omega_d(t)/dt\} + \hat{w}_2(t)v_c \tag{3}$$

where $\omega_d(t)$ is the desired output, $\omega_d(t)$ and $d\omega_d(t)/dt$ are both bounded, and v_c is a constant. The first two terms represent the adaptive feedforward control action for the desired output, and the third term represents that for the disturbance input. $\hat{w}_i(t)$'s are adjusted by the adaptation law,

$$\begin{aligned} d\hat{w}_0(t)/dt &= \gamma\, \omega_d(t)e(t) \\ d\hat{w}_1(t)/dt &= \gamma\{d\omega_d(t)/dt\}e(t) \\ d\hat{w}_2(t)/dt &= \gamma v_c e(t) \end{aligned} \tag{4}$$

where γ is a positive adaptation gain.

By defining,

$$\hat{\theta}(t)^T = [\hat{w}_0(t)\ \ \hat{w}_1(t)\ \ \hat{w}_2(t)]$$

and

$$\phi(t)^T = [\omega_d(t)\ \ d\omega_d(t)/dt\ \ v_c],$$

the adaptation law can be written as

$$d\hat{\theta}(t)/dt = \gamma\, \phi(t)\, e(t) \tag{5}$$

Under the assumption that the nonadaptive feedback control loop consisting of the plant and proportional controller remains asymptotically stable, the disturbance (d) is constant, and the desired output and its derivative are bounded, it can be shown that the overall adaptive system is stable and the tracking error converges to zero asymptotically (see Appendix A for details). Notice that when the error is zero, i.e. $e(t) = 0$, the motor is purely under feedforward control.

If we apply this adaptive feedforward controller to each axis control in a two axes problem, the overall system becomes as shown in Fig. 2. The adaption law for each axis is

$$d\hat{\theta}_i(t)/dt = \gamma\, \phi_i(t)\, e_i(t); \quad i = 1 \text{ or } 2$$

For a step disturbance input applied to the second axis, the system responds as shown in Fig. 3. Notice that the error of the undisturbed axis remains zero, and the two axes are unsynchronized during the recovery process of the disturbed axis.

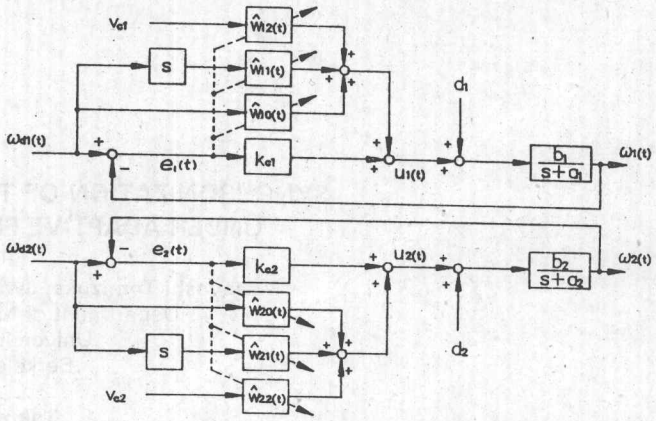

Fig. 2 Adaptive Feedforward Control for Two Axes System (Continuous Time)

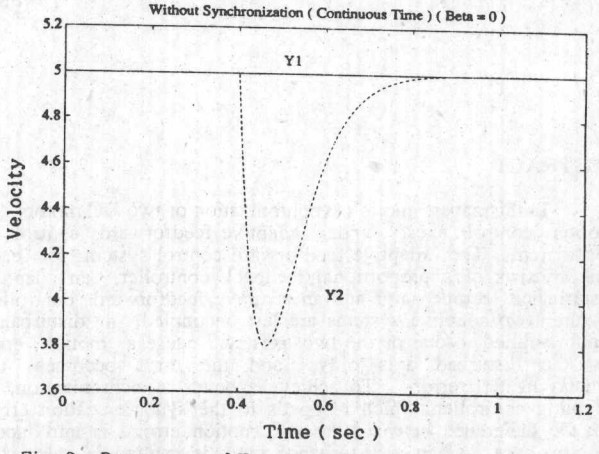

Fig. 3 Responses of Two Axes System to Step Disturbance (Independent Adaptive Feedforward Control)

Synchronization of Two Motion Control Axes

To achieve a better synchronization, we measure the differential error,

$$\varepsilon(t) = e_1(t) - e_2(t) \tag{6}$$

and modify the overall control structure in Fig. 2 to the one in Fig. 4. Notice that the additional coupling controller increases an effective loop gain for each axis. The parameter adaptation law is modified to

$$d\hat{\theta}_1(t)/dt = \gamma\, \phi_1(t)\, [e_1(t) + \beta\varepsilon(t)] \tag{7}$$

$$d\hat{\theta}_2(t)/dt = \gamma\, \phi_2(t)\, [e_2(t) - \beta\varepsilon(t)] \tag{8}$$

where the adaptation gain γ is any positive number and the positive coupling parameter β must be selected so that

$$\begin{bmatrix} a_1/b_1 + (1+\beta)k_{c1} & -(1/2)\beta(k_{c1} + k_{c2}) \\ -(1/2)\beta(k_{c1} + k_{c2}) & a_2/b_2 + (1+\beta)k_{c2} \end{bmatrix}$$

is positive definite (9)

In particular, if two axes possess identical dynamics, i.e. $a_1 = a_2$, $b_1 = b_2$ and $k_{c1} = k_{c2}$, β can take any positive value.

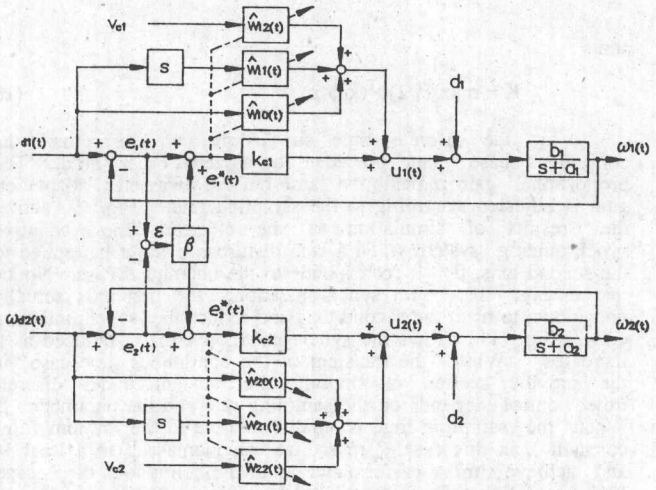

Fig. 4 Synchronized Adaptive Feedforward Control for Two Axes System (Continuous Time)

Notice that the synchronization error, ε, drives the two parameter vectors, $\hat{\theta}_1(t)$ and $\hat{\theta}_2(t)$, in opposite directions, which results in faster removal of the synchronization error. Fig. 5 shows the results of simulation of this adaptive synchronizing system when a step disturbance input is applied to the second axis. Notice that the errors appear both in the first and second axes but that the synchronization error is quickly removed. As shown in Fig. 6, the synchronization error is significantly reduced as the coupling parameter in the controller, β, is increased. The stability proof for this adaptive synchronizing control system is similar to but more tedious than that of the single axis adaptive feedforward control system (see Appendix B for details).

ADAPTIVE SYNCHRONIZING CONTROL — DISCRETE TIME CASE

The adaptive synchronizing control scheme presented in the previos section is a continuous time scheme. Since the implementation of a continuous time controller requires analog devices and is usually inconvenient, it is of practical interest to implement the control algorithm using digital computers. In the digital implementation, the stability conditions are in general dirrerent from those for the continuous time system because of the sampling effect. In this section, we will consider a discrete time formulation of motion synchronization. A sufficient condition that guarantees the stability of the discrete time problem is presented.

Adaptive Feedforward Control

When the first order system of Eq. (1) is under digital control, the input-output discrete time transfer function model is

$$G(z) = b_d/(z - a_d) \tag{10}$$

where a_d and b_d are related to the parameters of the continuous time model by

$$a_d = e^{-aT},\ b_d = (b/a)(1 - e^{-aT}),\ \text{and T = sampling period}$$

Notice that the plant parameters satisfy

$$0 < a_d < 1 \quad \text{and} \quad b_d > 0$$

The overall control system is configured as shown in Fig. 7. The proportional feedback control gain is selected so that

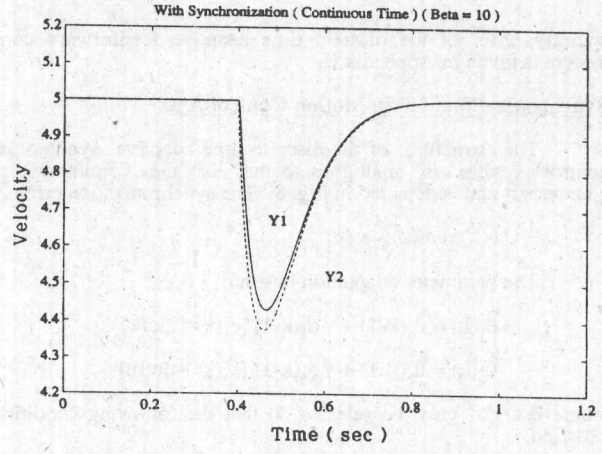

Fig. 5 Responses of Two Axes System to Step Disturbance (Synchronized Adaptive Feedforward Control)

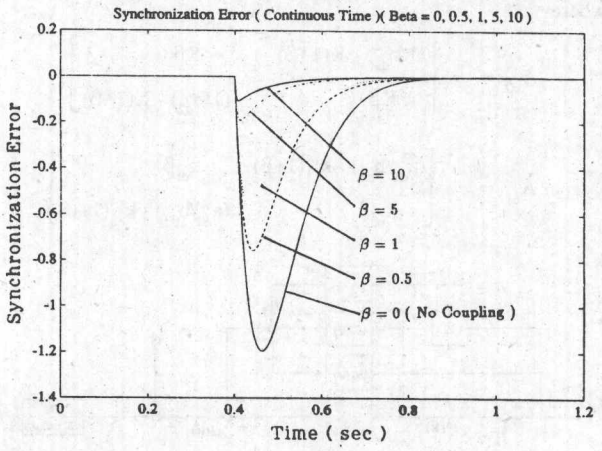

Fig. 6 Effect of Coupling Parameter (ß) on Synchronization Error (Continuous Time)

$$0 < a_d - b_d k_c < a_d,\quad k_c > 0$$

The feedforward control input is

$$u_f(k) = \hat{w}_0(k)\omega_d(k) + \hat{w}_1(k)\omega_d(k+1) + \hat{w}_2(k)v_c$$
$$= \hat{\theta}(k)^T\phi(k) \tag{11}$$

where

$$\hat{\theta}(k)^T = [\hat{w}_0(k)\ \ \hat{w}_1(k)\ \ \hat{w}_2(k)]$$

and

$$\phi(k)^T = [\omega_d(k)\ \ \omega_d(k+1)\ \ v_c],$$

The parameter adaptation algorithm is

$$\hat{\theta}(k) = \hat{\theta}(k-1) + \gamma\,\phi(k-1)\,e(k) \tag{12}$$

where γ is selected so that

$$(\gamma/2)\|\phi(k-1)\|^2 = (\gamma/2)\phi^T(k-1)\phi(k-1) < (1/b_d)[1 - (a_d - b_d k_c)] \tag{13}$$

Notice that Eq. (13) limits the value of the adaptation gain. In the continuous time case, γ was any positive number. The

stability proof of the discrete time adaptive feedforward control system is given in Appendix C.

Synchronization of Two Motion Control Axes

The structure of the discrete time adaptive synchronizing control system is analogous to that of the continuous time counterpart and is depicted in Fig. 8. The synchronization error is

$$\varepsilon(k) = e_1(k) - e_2(k) \tag{14}$$

The parameter adaptation law is

$$\hat{\theta}_1(k) = \hat{\theta}_1(k-1) + \gamma\,\phi_1(k-1)\,[e_1(k) + \beta\varepsilon(k)] \tag{15}$$

$$\hat{\theta}_2(k) = \hat{\theta}_2(k-1) + \gamma\,\phi_2(k-1)\,[e_2(k) - \beta\varepsilon(k)] \tag{16}$$

where β and γ must be selected so that the following condition is satisfied.

$$[A_{c0} - A_{c1}z^{-1}]^{-1} \text{ is strictly positive real} \tag{17}$$

where

$$A_{c0} = \begin{bmatrix} (1/b_{d1}) - K(1+\beta) & K\beta \\ K\beta & (1/b_{d2}) - K(1+\beta) \end{bmatrix}$$

$$A_{c1} = \begin{bmatrix} (a_{d1}/b_{d1}) - k_{c1}(1+\beta) & k_{c1}\beta \\ k_{c2}\beta & (a_{d2}/b_{d2}) - k_{c2}(1+\beta) \end{bmatrix}$$

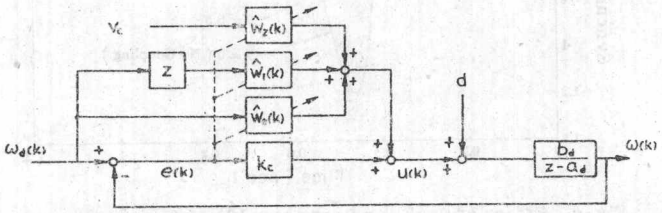

Fig. 7 Adaptive Feedforward Control System (Discrete Time)

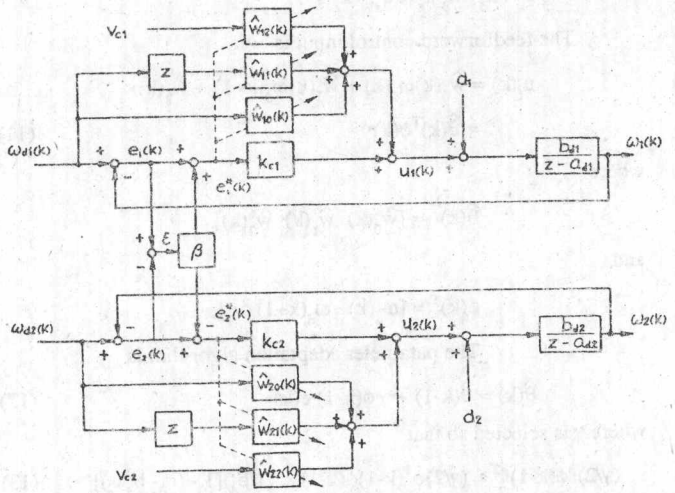

Fig. 8 Synchronized Adaptive Feedforward Control for Two Axes System (Discrete Time)

and

$$K = \max_k(\gamma/2)\phi^T(k)\phi(k) \tag{18}$$

In the discrete time simulation, we discretize the continuous case plant preceded by a zero order hold. The proportional gain remains the same but the parameter adaptation gain is adjusted according to the sampling rate. Fig. 9 shows the results of simulation of the discrete time adaptive synchronizing system when a step disturbance input is applied to the second axis. $\beta = 0$ corresponds to the uncoupled case. Notice that in Fig. 10, with synchronization, the first axis actually goes down to meet the second axis and reduce the synchronization error. Fig. 11 shows the synchronization error is reduced as β increases. While the transient of the continuous time case in the previous section was smooth, the transient under discrete time control depends on the sampling rate and the parameter β. When the sampling time is small (relative to the system time constant), in this case, 2 msec, we can increase β to a least 10 and achieve similar performance as in the continuous time case. If the sampling time is large, e.g. 10 msec, we can only increase β to around 3. As shown in Fig. 12 to 14, for β larger than 3 the transient becomes oscillatory and near instability as β is closer to 4.

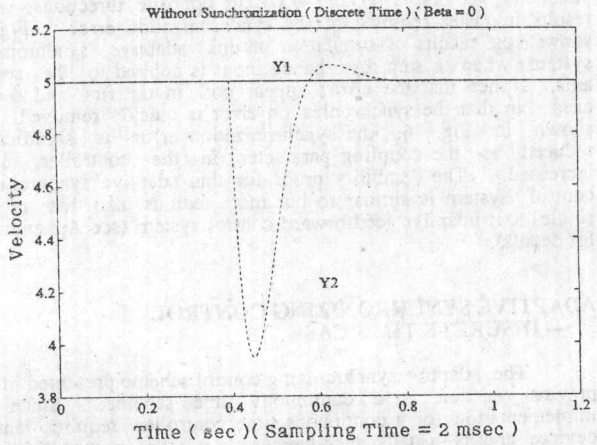

Fig. 9 Responses of Two Axes System to Step Disturbance (Independent Adaptive Feedforward Control – Discrete Time)

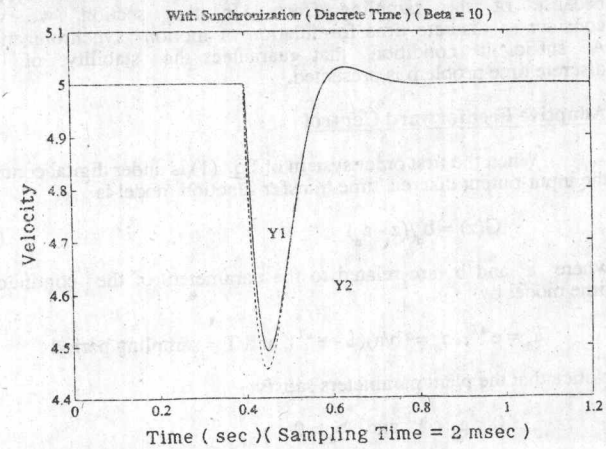

Fig.10 Responses of Two Axes System to Step Disturbance (Synchronized Adaptive Feedforward Control – Discrete Time)

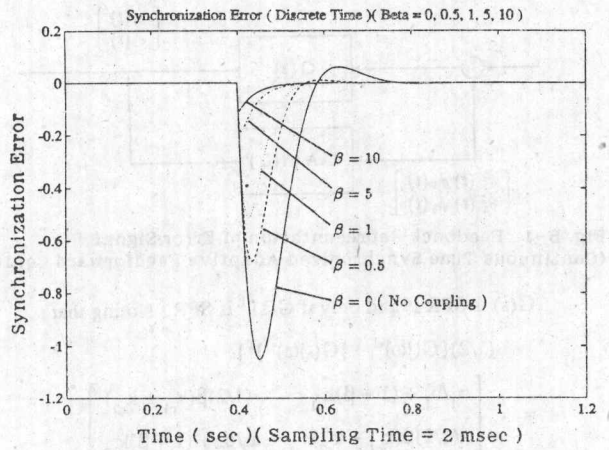

Fig.11 Effect of Coupling Parameter (ß) on Synchronization Error (Discrete Time)

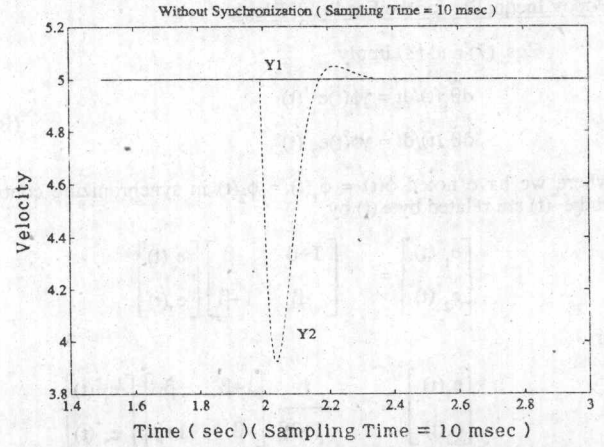

Fig.12 Effect of Sampling Time in Disturbance Rejection (Independent Adaptive Feedforward Control - Discrete Time)

CONCLUDING REMARKS

The adaptive synchronizing approach has been proposed for two axes velocity control systems. Each axis was under proportional feedback control and adaptive feedforward control. The stability of adaptive synchronizing system was investigated both in the continuous time domain and the discrete time domain. Simulation results demonstrated the effectiveness of the proposed approach. The extension of this approach to position control problem is straightforward.

REFERENCES

Landau, Y., (1979), Adaptive Control: The Model Reference Approach, Marcel Dekker

Koren, Y., (1980), "Cross-Coupled Biaxial Computer Controls for Manufacturing Systems," ASME Journal of Dynamic Systems, Measurement and Control, Vol. 102, pp. 265-272, 1980.

Tomizuka, M., (1989), "Design of Digital Tracking Controllers for Manufacturing Applications," Manufacturing Review, Vol. 2, No. 2, June 1989, pp. 134-141 (ASME)

Uchiyama, M. and Nakamura, Y., (1988), "Symmetric Hybrid Position/Force Control of Two Cooperating Robot Manipulators," Proceedings of 1988 IEEE International Workshop on Intelligent Robots and Systems, pp. 515-520, Nov. 1988.

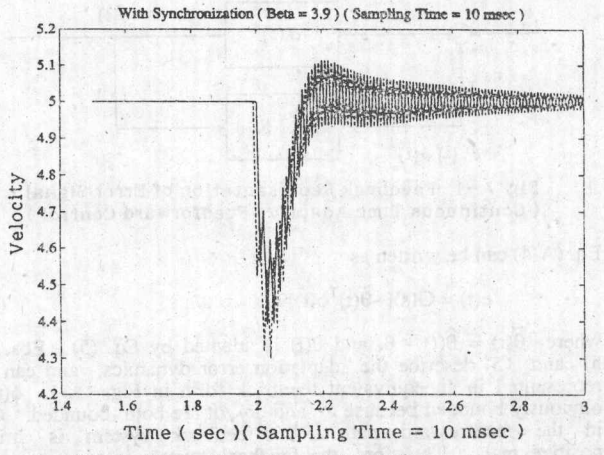

Fig.13 Effect of Sampling Time in Disturbance Rejection (Synchronized Adaptive Feedforward Control - Discrete Time)

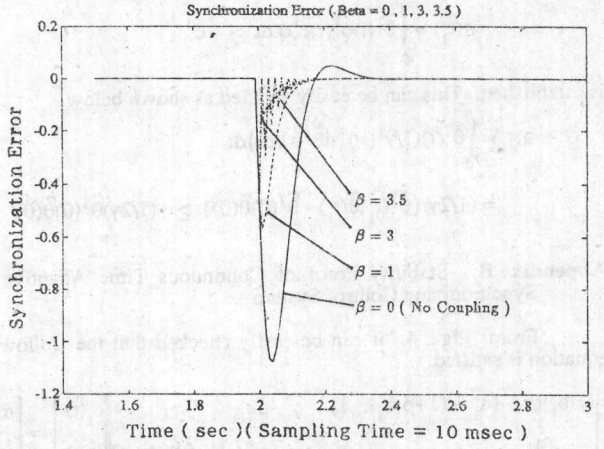

Fig.14 Effect of Coupling Parameter (ß) on Synchronization Error (Discrete Time)

Appendix A: Stability Proof of Continuous Time Adaptive Feedforward Control System

Stability proofs in appendices are all based on hyperstability (e.g. Landau, 1979). Note the following relations among signals in Fig. 1.

$$e(t) = \omega_d(t) - \omega(t) \tag{A-1}$$

$$d\omega(t)/dt + a\,\omega = b\,[k_c e(t) + u_f(t) + d] \tag{A-2}$$

$$u_f(t) = \hat{w}_0(t)\omega_d(t) + \hat{w}_1(t)\{d\omega_d(t)/dt\} + \hat{w}_2(t)v_c \tag{A-3}$$

From Eqs. (A-1) - (A-3),

$$\{(a + bk_c)e(t) + de(t)/dt\}/b$$

$$= (a/b - \hat{w}_0(t))\omega_d + (1/b - \hat{w}_1(t))d\omega_d/dt + (-d/v_c - \hat{w}_2(t))v_c \tag{A-4}$$

By defining,

$$G(s) = b/\{s + (a + k_c b)\}$$

$$\theta^T = [a/b \;\; 1/b \;\; -d/v_c],$$

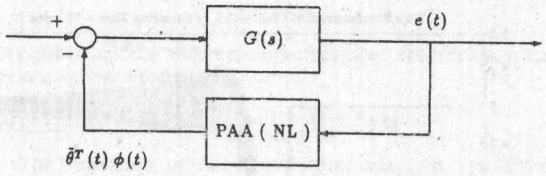

Fig. A−1 Feedback Representation of Error Signal (Continuous Time Adaptive Feedforward Control)

Eq. (A-4) can be written as

$$e(t) = G(s)[\,-\tilde{\theta}(t)^T\phi(t)] \tag{A-5}$$

where $\tilde{\theta}(t) = \hat{\theta}(t) - \theta$, and $\theta(t)$ is adapted by Eq. (5). Eqs. (A-5) and (5) describe the adaptation error dynamics, and can be represented in an equivalent feedback form in Fig. A-1. $\phi(t)$ is obviously bounded because ω_d and $d\omega_d/dt$ are both bounded. G(s) in the feedforward path of this feedback system is strictly positive real. Therefore, the feedback system is asymptotocally stable if the Popov inequality,

$$\eta(t_1) = \int_0^{t_1} \tilde{\theta}^T(t)\phi^T(t)e(t)\,dt \geq -c^2$$

is established. This can be easily verified as shown below.

$$\eta(t_1) = \int_0^{t_1} \tilde{\theta}^T(t)(1/\gamma^T(t))\{d\tilde{\theta}^T(t)/dt\}dt$$

$$= (1/2\gamma)\{\tilde{\theta}^T(t_1)\tilde{\theta}(t_1) - \tilde{\theta}^T(0)\tilde{\theta}(0)\} \geq -(1/2\gamma)\tilde{\theta}^T(0)\tilde{\theta}(0)$$

Appendix B: Stability Proof of Continuous Time Adaptive Synchronizing Control System

From Fig. 4, it can be easily checked that the following equation is satified.

$$\begin{bmatrix} (1/b_1)[s + \{a_1 + (1+\beta)b_1k_{c1}\}] & -\beta k_{c1} \\ -\beta k_{c2} & (1/b_2)[s + \{a_2 + (1+\beta)b_2k_{c2}\}] \end{bmatrix} \begin{bmatrix} e_1(t) \\ e_2(t) \end{bmatrix} = \begin{bmatrix} m_1(t) \\ m_2(t) \end{bmatrix} \tag{B-1}$$

where

$$\begin{bmatrix} m_1(t) \\ m_2(t) \end{bmatrix} = - \begin{bmatrix} \tilde{\theta}_1^T(t)\phi_1(t) \\ \tilde{\theta}_2^T(t)\phi_2(t) \end{bmatrix} \tag{B-2}$$

$\tilde{\theta}_i(t)$ is defined by

$$\tilde{\theta}_i(t) = \hat{\theta}_i(t) - \theta_i \tag{B-3}$$

where

$$\theta_i^T = [a_i/b_i \quad 1/b_i \quad -d/v_{ci}]$$

Eqs. (B-1) and (B-2) can be represented by the feedback system in Fig. B-1. G(s) in Fig. B-1 is

$$G(s) = \begin{bmatrix} (1/b_1)[s + \{a_1 + (1+\beta)b_1k_{c1}\}] & -\beta k_{c1} \\ -\beta k_{c2} & (1/b_2)[s + \{a_2 + (1+\beta)b_2k_{c2}\}] \end{bmatrix}^{-1} \tag{B-4}$$

This feedback system is asymptotically stable if G(s) is strictly positive real (SPR) and the feedback block satisfies the Popov inequality.

SPR Condition for G(s)

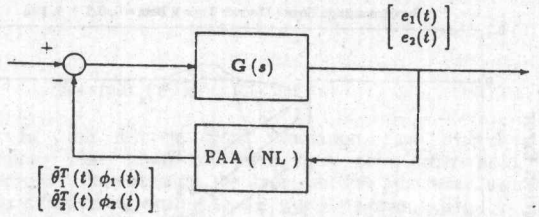

Fig. B−1 Feedback Representation of Error Signal (Continuous Time Synchronized Adaptive Feedforward Control)

G(s) is SPR if and only if $G(s)^{-1}$ is SPR. Noting that

$$(1/2)\{G(j\omega)^{-1} + [G(-j\omega)^{-1}]^T\}$$

$$= \begin{bmatrix} a_1/b_1 + (1+\beta)k_{c1} & -(1/2)\beta(k_{c1} + k_{c2}) \\ -(1/2)\beta(k_{c1} + k_{c2}) & a_2/b_2 + (1+\beta)k_{c2} \end{bmatrix}$$

G(s) is SPR under the condition given by (9).

Popov Inequality for the Feedback Block

Eqs. (7) and (8) imply

$$\begin{aligned} d\tilde{\theta}_1(t)/dt &= \gamma\phi(t)e_1^*(t) \\ d\tilde{\theta}_2(t)/dt &= \gamma\phi(t)e_2^*(t) \end{aligned} \tag{B-5}$$

where we have noted $\phi(t) = \phi_1(t) = \phi_2(t)$ in synchronizing control and $e_i^*(t)$ are related by $e_i(t)$ by

$$\begin{bmatrix} e_1^*(t) \\ e_2^*(t) \end{bmatrix} = \begin{bmatrix} 1+\beta & -\beta \\ -\beta & 1+\beta \end{bmatrix} \begin{bmatrix} e_1(t) \\ e_2(t) \end{bmatrix}$$

or

$$\begin{bmatrix} e_1(t) \\ e_2(t) \end{bmatrix} = \frac{1}{1+2\beta} \begin{bmatrix} 1+\beta & \beta \\ \beta & 1+\beta \end{bmatrix} \begin{bmatrix} e_1^*(t) \\ e_2^*(t) \end{bmatrix}$$

The Popov inequality for the feedback block is established as shown below.

$$\int_0^{t_1} [\tilde{\theta}_1^T(t)\phi(t)\ \ \tilde{\theta}_2^T(t)\phi(t)] \begin{bmatrix} e_1(t) \\ e_2(t) \end{bmatrix} dt$$

$$= (1/1+2\beta)\int_0^{t_1} \tilde{\theta}_1^T(t)\{(1+\beta)\phi(t)e_1^*(t) + \beta\phi(t)e_2^*(t)\}$$
$$+ \tilde{\theta}_2^T(t)\{\beta\phi(t)e_1^*(t) + (1+\beta)\phi(t)e_2^*(t)\beta\phi e_1^*(t)\}dt$$

$$= (1/1+2\beta)\int_0^{t_1} \tilde{\theta}_1^T(t)\{((1+\beta)/\gamma)[d\tilde{\theta}_1(t)/dt] + (\beta/\gamma)[d\tilde{\theta}_2(t)/dt]\}$$
$$+ \tilde{\theta}_2^T(t)\{(\beta/\gamma)[d\tilde{\theta}_1(t)/dt] + ((1+\beta)/\gamma)[d\tilde{\theta}_2(t)/dt]\}dt$$

$$= (1/1+2\beta)[\{(1+\beta)/(2\gamma)\}\{\tilde{\theta}_1^T(t_1)\tilde{\theta}_1(t_1) - \tilde{\theta}_1^T(0)\tilde{\theta}_1(0)\}$$
$$+ \{(1+\beta)/(2\gamma)\}\{\tilde{\theta}_2^T(t_1)\tilde{\theta}_2(t_1) - \tilde{\theta}_2^T(0)\tilde{\theta}_2(0)\}$$
$$+ \{\beta/\gamma\}\{\tilde{\theta}_1^T(t_1)\tilde{\theta}_2(t_1) - \tilde{\theta}_1^T(0)\tilde{\theta}_2(0)\}]$$

$$\geq -(1/2\gamma)\tilde{\theta}_1^T(0)\tilde{\theta}_1(0)$$
$$-(1/2\gamma)\tilde{\theta}_2^T(0)\tilde{\theta}_2(0) - (\beta/2\gamma)\{\tilde{\theta}_1(0) + \tilde{\theta}_2(0)\}^T\{\tilde{\theta}_1(0) + \tilde{\theta}_2(0)\}.$$

(End of Proof)

Appendix C: Stability of Discrete Time Adaptive Feedforward Control System

From Fig. 7, it can be easily checked that the following equation is satisfied,

$$e(k) = \{b_d z/[z - (a_d - b_d k_c)]\}\{-\tilde{\theta}^T(k-1)\phi(k-1)\} \qquad \text{(C-1)}$$

where

$$\tilde{\theta}(k) = \hat{\theta}(k) - \theta$$

and θ is given by

$$\theta^T = [-a_d/b_d \;\; -1/b_d \;\; -d/v_c]$$

From Eq. (12),

$$\tilde{\theta}(k) = \tilde{\theta}(k-1) + \gamma\phi(k-1)e(k) \qquad \text{(C-2)}$$

Eq. (C-1) can be represented by the feedback system in Fig. C-1a. We rearrange this feedback sytem as shown in Fig. C-1b. The feedback system in Fig. C-1a is asymptotically stable if and only if the one in Fig. C-1b is asymptotically stable. The transfer function of the linear block in Fig. C-1b is

$$b_d/[(1-Kb_d) - (a_d - b_d k_c)z^{-1}] \qquad \text{(C-3)}$$

For K>0, this transfer function is strictly positive real as long as

$$(a_d - b_d k_c)/(1 - Kb_d) < 1$$

or

$$K < (1/b_d)[1 - (a_d - b_d k_c)] \qquad \text{(C-4)}$$

From Eq. (C-2),

$$\tilde{\theta}(k-1) = \gamma \sum_{j=0}^{k-1} \phi(j-1)e(j) + \tilde{\theta}(0)$$

The summation of the input-output products of the feedback block in Fig. C-1b is

$$\eta(k_1) = \sum_{k=0}^{k_1} [\gamma \sum_{j=0}^{k-1} \phi(j-1)e(j) + \tilde{\theta}(0)]\phi(k-1) + Ke(k)]e(k)$$

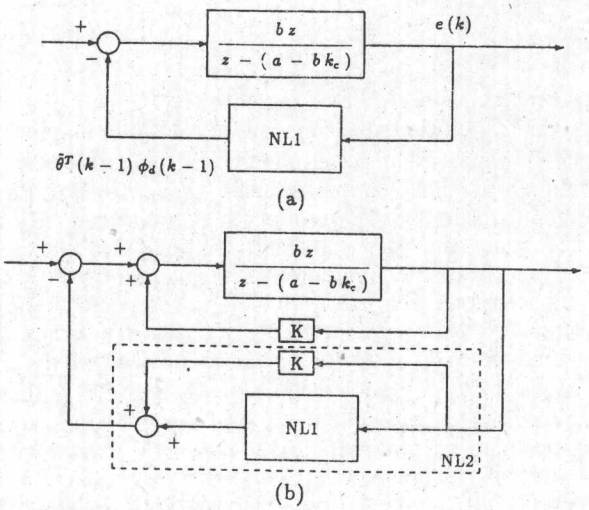

Fig. C-1 Feedback Representation of Error Signal (Discrete Time Adaptive Feedforward Control)

$$= (1/2\gamma)\tilde{\theta}^T(k_1)\tilde{\theta}(k_1) + \sum_{k=0}^{k_1}\{K - (\gamma/2)\phi^T(k-1)\phi(k-1)\}e^2(k) - (1/2\gamma)\tilde{\theta}^T(0)\tilde{\theta}(0)$$

Notice that $\eta(k_1)$ is lower bounded by $-(1/2\gamma)\tilde{\theta}^T(0)\tilde{\theta}(0)$ if

$$K - (\gamma/2)\phi^T(k-1)\phi(k-1) \geq 0 \qquad \text{(C-5)}$$

Therefore the feedback block satisfies the Popov inequality if (C-5) is satified. From Eqs. (C-4) and (C-5), the feedback system is asymptotically stable for γ satifying Eq. (13).
(End of Proof)

Appendix D: Stability of Discrete Time Adaptive Synchronizing Control System

From Fig. 8, it can be checked that the following equation is satisfied.

$$[I - A_1 z^{-1}]\begin{bmatrix} e_1(k) \\ e_2(k) \end{bmatrix} = B_0 \begin{bmatrix} -\tilde{\theta}_1^T(k-1)\phi_1(k-1) \\ -\tilde{\theta}_2^T(k-1)\phi_2(k-1) \end{bmatrix} \qquad \text{(D-1)}$$

where I is a 2x2 identity matrix,

$$A_1 = \begin{bmatrix} a_{d1} - b_{d1}k_{c1}(1+\beta) & b_{d1}k_{c1}\beta \\ b_{d2}k_{c2}\beta & a_{d2} - b_{d2}k_{c2}(1+\beta) \end{bmatrix} \qquad B_0 = \begin{bmatrix} b_{d1} & 0 \\ 0 & b_{d2} \end{bmatrix}$$

$$\tilde{\theta}_i(k) = \hat{\theta}_i(k) - \theta_i$$

$$\theta_i = [-a_{di}/b_{di} \;\; -1/b_{di} \;\; -d_i/v_{ci}]$$

Eq.(D-1) can be represented by the feedback system in Fig. D-1a, which can be further rearranged as shown in Fig. D-1b. The stability is considered for the rearranged form in Fig. D-1b. The transfer function matrix of the linear block in Fig. D-1b is

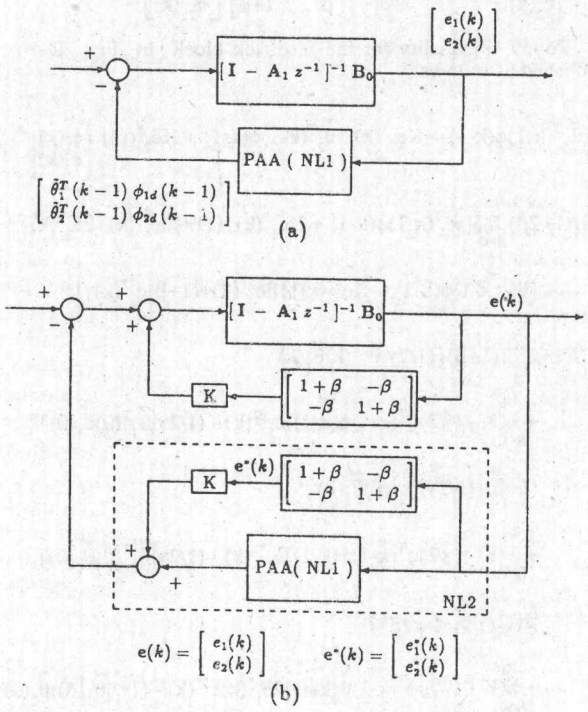

Fig. D-1 Feedback Representation of Error Signal (Discrete Time Synchronized Adaptive Feedforward Control)

$$[A_{c0} - A_{c1}z^{-1}]^{-1} \qquad \text{(D-2)}$$

where

$$A_{c0} = \begin{bmatrix} (1/b_{d1}) - K(1+\beta) & K\beta \\ K\beta & (1/b_{d2}) - K(1+\beta) \end{bmatrix}$$

$$A_{c1} = \begin{bmatrix} (a_{d1}/b_{d1}) - k_{c1}(1+\beta) & k_{c1}\beta \\ k_{c2}\beta & (a_{d2}/b_{d2}) - k_{c2}(1+\beta) \end{bmatrix}$$

β and K must be selected so that $\mathbf{G}(z)$ in Eq. (D-2) is strictly positive real, which is the stated condition in 3.2. It will be shown below that the feedback block in Fig. D-1b satisfies the Popov inequality under Eq. (18). Therefore, the feedback system is asymptotically stable when the condition stated by (17) and (18) is saisfied.

Popov inequality

Eqs. (15) and (16) imply

$$\tilde{\theta}_1(k) = \tilde{\theta}_1(k-1) + \gamma\,\phi_1(k-1)e_1^*(k)$$

$$\tilde{\theta}_2(k) = \tilde{\theta}_2(k-1) + \gamma\,\phi_2(k-1)e_2^*(k)$$

where we have noted $\phi(k-1) = \phi_1(k-1) = \phi_2(k-1)$ in synchronizing control, and $e_i^*(k)$ are related to $e_i(k)$ by

$$\begin{bmatrix} e_1^*(k) \\ e_2^*(k) \end{bmatrix} = \begin{bmatrix} 1+\beta & -\beta \\ -\beta & 1+\beta \end{bmatrix} \begin{bmatrix} e_1(k) \\ e_2(k) \end{bmatrix}$$

or

$$\begin{bmatrix} e_1(k) \\ e_2(k) \end{bmatrix} = \frac{1}{1+2\beta} \begin{bmatrix} 1+\beta & \beta \\ \beta & 1+\beta \end{bmatrix} \begin{bmatrix} e_1^*(k) \\ e_2^*(k) \end{bmatrix}$$

The Popov inequality for the feedback block in Fig. D-1b is established as follows.

$$\sum_{k=0}^{k_1} [\tilde{\theta}_1^T(k-1)\phi(k-1) + Ke_1^*(k) \;\; \tilde{\theta}_2^T(k-1)\phi(k-1) + Ke_2^*(k)] \begin{bmatrix} e_1(k) \\ e_2(k) \end{bmatrix}$$

$$= 1/(1+2\beta) \sum_{k=0}^{k_1} [\{\tilde{\theta}_1^T(k-1)\phi(k-1) + Ke_1^*(k)\}\{(1+\beta)e_1^*(k)+\beta e_2^*(k)\}$$

$$\{\tilde{\theta}_2^T(k-1)\phi(k-1) + Ke_2^*(k)\}\{\beta e_1^*(k)+(1+\beta)e_2^*(k)\}]$$

$$= 1/(1+2\beta)[(1+\beta)\{(1/2\gamma)\tilde{\theta}_1^T(k)\tilde{\theta}_1(k)$$

$$+ \sum_{k=0}^{k_1}(K - (\gamma/2)\phi^T(k-1)\phi(k-1))e_1^{*2}(k) - (1/2\gamma)\tilde{\theta}_1^T(0)\tilde{\theta}_1(0)\}$$

$$(1+\beta)\{(1/2\gamma)\tilde{\theta}_2^T(k)\tilde{\theta}_2(k)$$

$$+ \sum_{k=0}^{k_1}(K - (\gamma/2)\phi^T(k-1)\phi(k-1))e_2^{*2}(k) - (1/2\gamma)\tilde{\theta}_2^T(0)\tilde{\theta}_2(0)\}$$

$$\beta\{(1/\gamma)\tilde{\theta}_1^T(k)\tilde{\theta}_2(k)$$

$$+ \sum_{k=0}^{k_1}(K - (\gamma/2)\phi^T(k-1)\phi(k-1))2e_1^*(k)e_2^*(k) - (1/\gamma)\tilde{\theta}_1^T(0)\tilde{\theta}_2(0)\}]$$

$$\geq -(1/2\gamma)\tilde{\theta}_1^T(0)\tilde{\theta}_1(0)$$

$$- (1/2\gamma)\tilde{\theta}_2^T(0)\tilde{\theta}_2(0) - (\beta/2\gamma)\{\tilde{\theta}_1(0)+\tilde{\theta}_2(0)\}^T\{\tilde{\theta}_1(0)+\tilde{\theta}_2(0)\}.$$

where we have noted

$$K - (\gamma/2)\phi^T(k-1)\phi(k-1) \geq 0$$

$$\tilde{\theta}_1^T(k)\tilde{\theta}_1(k) + \tilde{\theta}_2^T(k)\tilde{\theta}_2(k) + 2\tilde{\theta}_1^T(k)\tilde{\theta}_2(k)$$

$$= (\tilde{\theta}_1(k)+\tilde{\theta}_2(k))^T(\tilde{\theta}_1(k)+\tilde{\theta}_2(k)) \geq 0$$

and $\quad e_1^{*2}(k) + e_2^{*2}(k) + 2e_1^*(k)e_2^*(k) = (e_1^*(k)+e_2^*(k))^2 \geq 0.$

(End of Proof)

AN EXPERIMENTAL INVESTIGATION OF TWO DIGITAL TRACKING CONTROLLERS: ADAPTIVE AND NON-ADAPTIVE

Anthony Smith and Kok-Meng Lee
Georgia Institute of Technology
The George W. Woodruff School of Mechanical Engineering
Atlanta, Georgia

ABSTRACT

An experimental investigation of two tracking controllers; one adaptive, the other non-adaptive; was performed on a three link in-parallel manipulator to compare their performance. Both controllers were challenged by the presence of modeling error, sensor noise and plant nonlinearities. The adaptive controller was an adaptive zero phase error tracking controller (AZPETC), the non-adaptive controller was a zero phase error tracking controller (ZPETC) used with a tracking error integrator. The overall performance of the adaptive controller was better than the non-adaptive controller's.

1 INTRODUCTION

The ability of robotic manipulators to track a desired trajectory is gaining importance, particularly in the area of machining. One controller that is good for this task is the zero phase error tracking controller (ZPETC) (Tomizuka, 1987). However, as with most feedforward controllers, the ZPETC is sensitive to modeling error.

This paper experimentally evaluates two approaches for reducing the model sensitivity of the ZPETC. The first, a non-adaptive controller, places a tracking error integrator in parallel with the ZPETC. The second, an adaptive controller, is the adaptive ZPETC (AZPETC) proposed by Tsao and Tomizuka (1987). The controllers were evaluated using a good and a poor model of the plant.

This paper also adds to the body of experimental data on adaptive controllers; they need to be implemented more often to determine their usefulness in practical situations. Some of the more recent experimental work was reported by Tomizuka, et al. (1988), Tsao and Tomizuka (1989), and Shi and Stelson (1989).

In the following section, the equipment setup is described. In section 3, the good model of the analog plant is derived. Section 4 reviews the ZPETC and AZPETC design, adds the integrator to the ZPETC design, and implements both controllers. The experimental results of both controllers using each plant model are presented in section 5. Conclusions are given in section 6.

Figure 1 Three link in-parallel manipulator

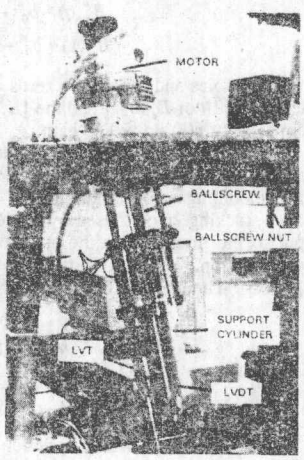

Figure 2 One link of the manipulator

2 EQUIPMENT SETUP

The experimental results presented in this paper were obtained on a three link in-parallel manipulator that has three degrees of freedom; it is shown in Figure 1. This manipulator has three extensible links, spaced 120 degrees apart from each other, that are attached to an upper stationary base platform by pin joints and to a lower moving platform by ball joints.

The setup of only one link will be discussed since the control algorithms evaluated are decentralized controllers. The main drive components of the link are labeled in Figure 2: motor, ballscrew, ballscrew nut and support cylinder. Also labeled is a linear variable differential transformer (LVDT) and a linear velocity transducer (LVT); these transducers provided feedback control signals. The equipment setup for the controllers is shown in Figure 3.

The motor used to drive each link is a low-inertia, copper-disc DC servomotor. This motor allows a higher peak current than conventional servomotors because it lacks iron laminations. The higher peak current rating results in a higher starting torque. The motor is directly coupled to the ballscrew. The ballscrew transforms rotary motion into linear motion and has a lead of 5 mm/revolution. The ballscrew nut is rigidly attached to the support cylinder. The support cylinder transfers power from the ballscrew nut to the lower base plate.

The LVDT was used by both controllers for digital position feedback. The signal was read by an A/D board; the quantization level was 43 microns.

The LVT was used by the plant for analog velocity feedback; this configuration makes the analog plant a velocity servo.

A current amplifier was used to power the DC motors. The current amplifier was an H-bridge amplifier and allowed four quadrant operation; the gain was 750 amps/volt. The amplifier has a bandwidth of

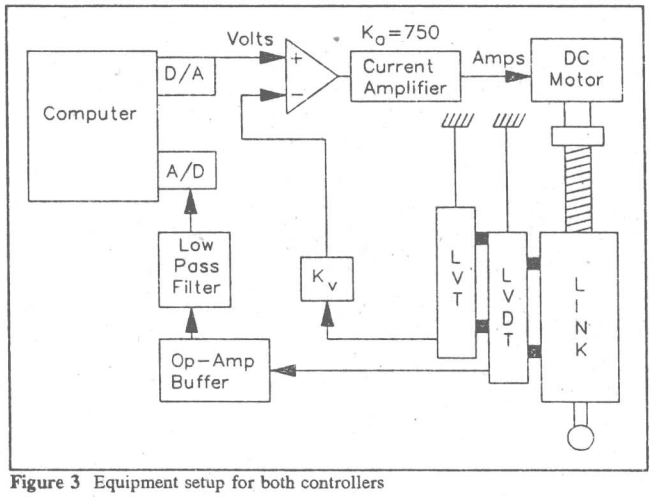

Figure 3 Equipment setup for both controllers

approximately 1 KHz; it was modeled as a pure gain. The amplifier was set for a maximum output of 30 amps for the first half second and 7.5 amps after 0.5 seconds.

The computer used to implement both digital controllers was a 12 MHz 80286 computer; it had a 12-bit 6 channel D/A board for output and a 12-bit 8 channel A/D board for input. The command signal of the digital controllers was output from the D/A board. This command voltage controlled the amount of current sent to the DC motor by the amplifier. The LVDT sensed the position of the link; an op-amp buffer and 100 Hz low pass filter were used to reduce the noise level of the signal. The A/D board read the filtered LVDT signal for use by the digital controllers.

3 MODEL OF ANALOG PLANT

The block diagram of the analog plant model is shown in Figure 4; the inner velocity feedback loop represents viscous damping present in the ballscrew assembly. The model parameters used are shown in Table 1. Using these parameters and referring to Figure 4, the analog plant transfer function is

$$G(s) = \frac{16359}{s(s+567)} \tag{1}$$

The high amplifier gain coupled with negative analog velocity feedback was used to compensate for the effects of Coulomb and static friction (Lee, Yien 1989).

For reasons to be explained shortly, when the AZPETC was used it was desirable for the closed-loop plant to be approximately first order. The velocity feedback gain, K_v, was adjusted to move the breakpoint of the digital root locus such that the faster plant pole approached the origin and became negligible. This value of K_v was used with both controllers so that a valid comparison of their performance could be made.

4 CONTROLLER DESIGN AND IMPLEMENTATION

4.1 ZPETC with Integral Control

The zero phase error tracking controller (ZPETC) is a digital feedforward algorithm for tracking time-varying trajectories that are known in advance (Tomizuka, 1987). The ZPETC uses a combination of

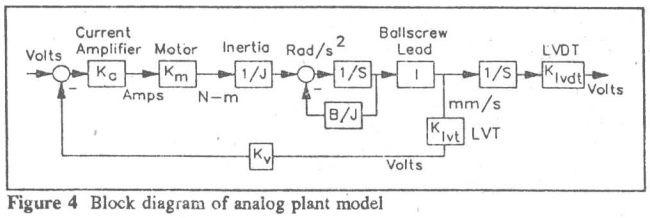

Figure 4 Block diagram of analog plant model

Table 1 - Model Parameters

Parameter	Symbol	Units	Value
Amplifier gain	K_a	Amps/Volt	38.0
Motor torque constant	K_m	N-m/Amp	0.17011
Ballscrew lead	l	mm/radian	0.7958
System inertia	J	N-m-s^2	2.4434 x 10^{-4}
LVDT gain	K_{lvdt}	mVolts/mm	58.5
LVT gain	K_{lvt}	mVolts/(mm/s)	17.52
Feedback gain	K_v	Dimensionless	0.0780
Viscous damping	B	(N-m)/(rad-s)	1.03 x 10^{-6}

pole/zero cancellation and phase cancellation to obtain good tracking. The plant poles and cancelable zeros are canceled; uncancelable zeros have their phase canceled. Uncancelable zeros are all of the non-minimum phase zeros and any zeros inside the unit circle that would cause a highly oscillatory output if inverted. The phase cancellation of the uncancelable zeros ensures that the system response has zero phase error for all frequencies.

Suppose that the closed-loop transfer function is given by

$$G_{closed}(q^{-1}) = \frac{q^{-d} B_c(q^{-1})}{A_c(q^{-1})} \tag{2}$$

where d is the relative degree of the plant, q^{-1} is a one step time delay operator and

$$B_c(q^{-1}) = b_0 + b_1 q^{-1} + \cdots + b_m q^{-m},\ b_0 \neq 0$$
$$A_c(q^{-1}) = 1 + a_1 q^{-1} + \cdots + a_n q^{-n}$$

To compensate for uncancelable zeros, $B_c(q^{-1})$ is factored into two parts so that

$$B_c(q^{-1}) = B_c^a(q^{-1}) B_c^u(q^{-1}) \tag{3}$$
$$\text{where}\quad B_c^u(q^{-1}) = b_0^u + b_1^u q^{-1} + \cdots + b_s^u q^{-s}$$

The $B_c^a(q^{-1})$ term contains the zeros that are cancelable; the $B_c^u(q^{-1})$ term contains the zeros that are uncancelable. Splitting $B_c(z^{-1})$ into two parts leads to the design of the ZPETC, which is

$$r(k) = \frac{A_c(q^{-1})\, B_c^u(q)}{B_c^a(q^{-1})\,[B_c^u(1)]^2}\, y_d(k+d) \tag{4}$$

where

$$B_c^u(q) = b_0^u + b_1^u q + \cdots + b_s^u q^s$$
$$B_c^u(1) = b_0^u + b_1^u + \cdots + b_s^u$$

The plant poles and cancelable zeros are canceled; the $B_c^u(q)$ term cancels the phase shift of $B_c^u(q^{-1})$ and the $[B_c^u(1)]^2$ term gives the transfer function from $y_d(k)$ to $y(k)$ unity DC gain.

If the plant dynamics are well known, the ZPETC works very well for trajectory control. However, the ZPETC is sensitive to modeling error. Since modeling error is ubiquitous, an integral controller was added to reduce tracking error caused by modeling error and/or disturbances. The input to the integrator is the error between the desired position and the plant position. The block diagram for this configuration is shown in Figure 5. The transfer function from $y_d(k)$ to $y(k)$ is

$$\frac{y(k)}{y_d(k)} = \frac{\left[\dfrac{B_c^u(q) B_c^u(q^{-1})}{B_c^u(1)^2}\right] A_c(q^{-1})(1-q^{-1}) + q^{-d} k_I B_c^a(q^{-1}) B_c^u(q^{-1})}{A_c(q^{-1})(1-q^{-1}) + q^{-d} k_I B_c^a(q^{-1}) B_c^u(q^{-1})} \tag{5}$$

If $k_I = 0$, then the transfer function is the same as that for the ZPETC only. Increasing k_I adds the same term to the numerator and denominator, but for small values of k_I the transfer function remains almost the same.

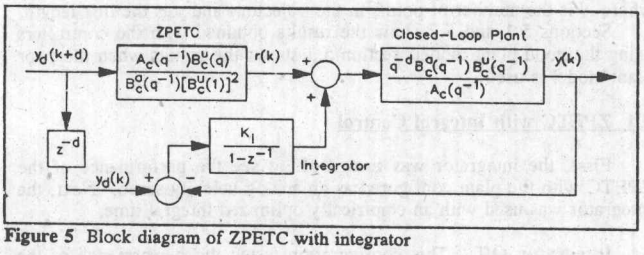

Figure 5 Block diagram of ZPETC with integrator

However, these small values of k_I are large enough to remove tracking error.

The ZPETC with integral control was implemented on the system shown in Figure 3. The transfer function for the plant is given in equation (1). The sampling period was 3 msec. Using zero-order hold equivalence, the discrete-time transfer function is

$$G(z^{-1}) = \frac{0.0449z^{-1}(1 + 0.5737z^{-1})}{(1 - z^{-1})(1 - 0.1822z^{-1})} \tag{6}$$

Digital position feedback was used to place the closed-loop plant poles; the slower pole was placed at 26 rad/sec. The closed-loop transfer function for the plant was

$$G_{cl}(z^{-1}) = \frac{3.673 \times 10^{-2} z^{-1}(1 + 0.5737z^{-1})}{(1 - 0.2196z^{-1})(1 - 0.9259z^{-1})} \tag{7}$$

The ZPETC was designed using equation (7). The $(1 + 0.5737z^{-1})$ term is on the negative real axis and would be highly oscillatory if inverted. Therefore, $B_c^u(z^{-1}) = (1 + 0.5737z^{-1})$ and $B_c^o(z^{-1}) = 3.673 \times 10^{-2}$. With the numerator factored this way, the ZPETC prefilter was

$$r(k) = 6.3060\,y(k+2) + 3.7692\,y(k+1) - 11.3100\,y(k) + 2.2348\,y(k-1) \tag{8}$$

The integrator was then tuned empirically to obtain the best system response.

4.2 Adaptive Zero Phase Error Tracking Controller

Another approach for solving the modeling error sensitivity of the ZPETC is to tune its coefficients in real time. The approach of Tsao and Tomizuka (1987) of using a parameter adaptation algorithm to tune the ZPETC coefficients was used here. The parameter adaptation algorithm (PAA) used was a normalized least squares adaptation algorithm.

The first step in designing the adaptive zero phase error tracking controller (AZPETC) is to separate the closed-loop system into a known part and an unknown part. The numerator of the known part is also divided into a cancelable and an uncancelable part so that

$$G_{closed}(q^{-1}) = \frac{y(k)}{y_m(k)} = \frac{q^{-d}B(q^{-1})B_0^-(q^{-1})B_0^+(q^{-1})}{A(q^{-1})A_0(q^{-1})} \tag{9}$$

where $A(q^{-1}) = 1 + a_1q^{-1} + \cdots + a_nq^{-n}$ is the unknown part and $A_0(q^{-1})$ is the known part of the denominator. $B(q^{-1}) = b_0 + b_1q^{-1} + \cdots + b_mq^{-m}$ is the unknown part of the numerator; the known part of the numerator is split into $B_0^-(q^{-1})$, $(B_0^-(1) \neq 0)$ and $B_0^+(q^{-1})$ which are the uncancelable and cancelable portions, respectively. The separation of the numerator and denominator into known and unknown parts is done to reduce the work required by the estimation algorithm; only the unknown part will be estimated.

Figure 6 shows the block diagram of the AZPETC. Referring to the figure, the reference model for the PAA is

$$y(k) = \frac{q^{-d}B(q^{-1})}{A(q^{-1})}r'(k) \tag{10}$$

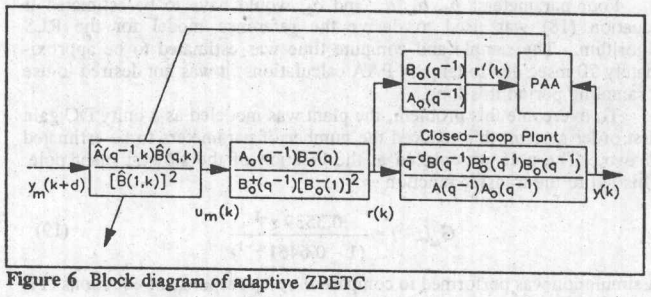

Figure 6 Block diagram of adaptive ZPETC

which can be written as

$$y(k+d) = \theta^T\phi(k)$$

$$\text{where} \quad \theta^T = (a_1, \ldots, a_n, b_0, \ldots, b_m) \tag{11}$$

$$\phi^T(k) = (-y(k+d-1), \ldots, -y(k+d-n), r'(k), \ldots, r'(k-m))$$

Let $n(k)$, $\phi(k)$ and $y(k)$ be defined by

$$n(k) = \max(\|\phi(k)\|, 1)$$

$$\phi(k) = \frac{\phi(k)}{n(k)} \tag{12}$$

$$y(k) = \frac{y(k)}{n(k)}$$

Normalization of the system inputs and outputs was performed to make the algorithm more numerically robust.

Using equations (12), the normalized least squares PAA for determining the unknown parameters in the AZPETC is

$$\hat{\theta}(k) = \hat{\theta}(k-1) + \frac{F(k-1)\,\phi(k-d)\,e^0(k)}{1 + \phi^T(k-d)\,F(k-1)\,\phi(k-d)} \tag{13}$$

where $e^o(k) = y(k) - \hat{\theta}^T(k-1)\,\phi(k-d)$ is the a priori adaptation error. The adaptation gain is adjusted by

$$F(k) = \frac{1}{\lambda(k)}\left[F(k-1) - \frac{F(k-1)\,\phi(k-d)\,\phi^T(k-d)F(k-1)}{1 + \phi^T(k-d)\,F(k-1)\,\phi(k-d)}\right] \tag{14}$$

where $\lambda(k)$ is the forgetting or exponential weighting factor.

With exponential weighting, $F(k)$ will rapidly approach $\underline{0}$ as the parameters converge. For time varying systems, it is desirable to always have the PAA ready to adapt to system changes. One way to do this is to keep the trace of $F(k)$ constant. The forgetting factor must be variable to do this and is adjusted by

$$\lambda(k) = 1 - \frac{1}{\text{tr}\,F(t=0)}\left[\frac{\phi^T(k-d)\,F^2(k-1)\,\phi(k-d)}{1 + \phi^T(k-d)\,F(k-1)\,\phi(k-d)}\right] \tag{15}$$

The AZPETC was implemented on the system shown in Figure 3. The transfer function for the plant is given in equation (1). The sampling period was 16.8 msec. Using zero-order hold equivalence, the discrete-time transfer function is

$$G(z^{-1}) = \frac{0.4335z^{-1}(1 + 0.1171z^{-1})}{(1 - z^{-1})(1 - 7.235 \times 10^{-5}z^{-1})} \tag{16}$$

Digital position feedback was used to place the closed-loop poles. As with the ZPETC with integral control, the slower closed-loop pole was placed at 26 rad/sec. The closed-loop transfer function for the plant was

$$G_{cl}(z^{-1}) = \frac{0.2995\,z^{-1}(1 + 0.1171\,Z^{-1})}{(1 - 0.0544\,z^{-1})(1 - 0.6461\,z^{-1})} \tag{17}$$

All the terms above have to be considered unknown parameters for the AZPETC algorithm since the coefficients depend on system parameters. Equation (17) is of the form

$$G_{cl}(z^{-1}) = \frac{z^{-d}(b_0 + b_1z^{-1})}{1 + a_1z^{-1} + a_2z^{-2}} \tag{18}$$

Four parameters; b_0, b_1, a_1, and a_2, would have to be estimated if equation (18) was used to derive the reference model for the RLS algorithm. The sample and compute time was estimated to be approximately 70 msec due to lengthy PAA calculations; it was not desired to use a sampling period this long.

To overcome this problem, the plant was modeled as a unity DC gain first order system; this reduced the number of parameters to be estimated to two. The pole was placed at the location of the slowest plant pole. This led to the transfer function

$$G_{cl}(z^{-1}) = \frac{0.3539\, z^{-1}}{(1 - 0.6461\, z^{-1})} \qquad (19)$$

A simulation was performed to compare the step response of equations (17) and (19); the two step responses were very similar.

Equation (19) is of the form

$$G_{cl}(z^{-1}) = \frac{z^{-d}\, b_0}{1 + a_1\, z^{-1}} \qquad (20)$$

Equation (20) was used to design the AZPETC prefilter. Both b_0 and a_1 are considered unknown; there is no known dynamics. Since there is no known dynamics, the AZPETC lacks a constant coefficient block (see Figure 6). This makes $r(k) = u_m(k)$. Also, the input to the reference model does not have to be prefiltered by known dynamics; this makes $r'(k) = r(k)$ (see Figure 6). Therefore, the AZPETC prefilter is

$$r(k) = \frac{1}{\hat{b}_0} \left[r(k+1) + \hat{a}_1\, r(k) \right] \qquad (21)$$

where $\hat{a}_1$ and $\hat{b}_0$ are parameter estimates provided by the RLS algorithm.

None of the methods mentioned by Tsao and Tomizuka (1987, 1989) to prevent parameter pathology or drift were incorporated in the AZPETC. However, simulations that included signal quantization and noise were performed to see if the AZPETC would work before implementing it; all of the simulations achieved parameter convergence.

5 EXPERIMENTAL RESULTS

To test the controllers' performance, a trajectory that represented the range of motion possible with the manipulator was created in Cartesian space. The location of the endpoint of the manipulator was described by one Cartesian degree of freedom and two orientation degrees of freedom. The trajectory was converted to the lengths for links 0, 1, and 2 using the inverse kinematics of the manipulator (Lee, Shah 1988). The link trajectory for link 0 is shown in Figure 7.

Only the results for link 0 will be shown; the results obtained on the other links were similar. To judge the performance of the controllers, the mean absolute error of the actual trajectories was used. The mean absolute error (MAE) was calculated using this algorithm:

$$\text{MAE} = \frac{1}{N} \sum_{n=1}^{N} \text{abs}(y_{desired} - y_{actual}) \qquad (22)$$

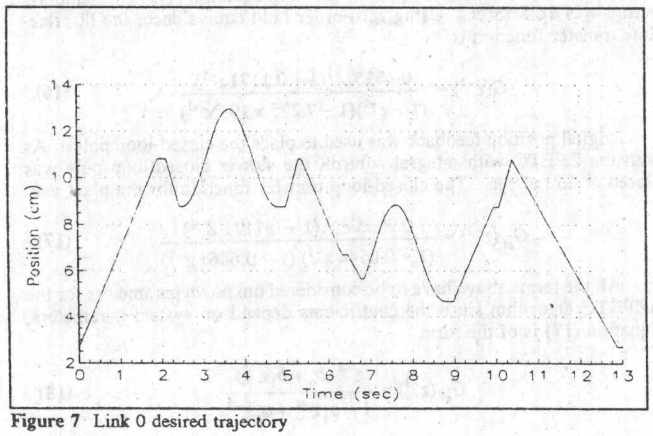

Figure 7 Link 0 desired trajectory

where N is the number of points in the trajectory and y is the link length.

Sections 5.1 and 5.2 show the results obtained with the controllers using the good plant model; section 5.3 shows the results when the poor plant model is used.

5.1 ZPETC with Integral Control

First, the integrator was turned off to see the performance of the ZPETC with the plant configured as an analog velocity servo. Next, the integrator was used with an empirically optimized integral time.

Integrator Off. This configuration tested the performance of the ZPETC with the plant configured as an analog velocity servo. The test had a MAE of 546.1 microns; the tracking error is shown in Figure 8. The inset in the tracking error plots is the desired trajectory.

The error in the trajectory is caused by modeling error; the actual path *leads* the desired path. The ZPETC is compensating for more phase shift than is necessary; the plant poles are faster than the modeled poles.

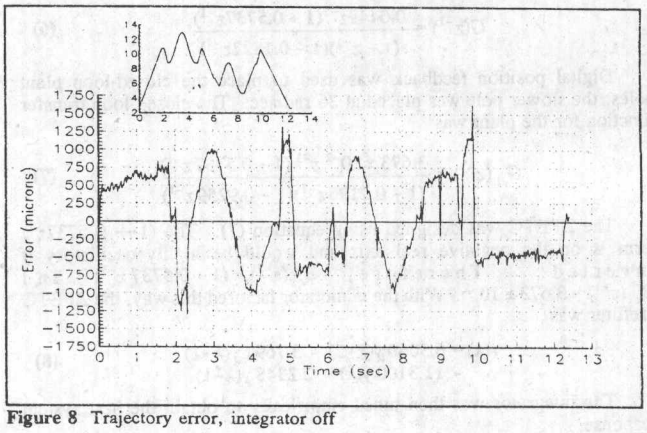

Figure 8 Trajectory error, integrator off

Integrator Operating. The integrator was then turned on to see if it would reduce the tracking error. The integral time was chosen empirically by following a trajectory using different integral times; the integral time with the lowest MAE ($T_i = 0.05$) was chosen. The results are shown in Table 2.

Table 2 - Integral Time versus MAE

Integral Time (sec)	MAE (microns)	
	Good model	Poor model
0.012	99.3	74.7
0.025	67.1	42.9
0.05	66.5	41.9
0.1	71.1	44.2
0.2	81.0	57.9

Table 2 shows that an integral time that is too short causes more error because of overshoot problems, an integral time that is too long does not remove tracking error fast enough.

The results of running the ZPETC with integral control with $T_i = 0.05$ are shown in Figures 9-a and 9-b. Figure 9-a shows the tracking error of the plant; the MAE was 111.8 microns. Figure 9-b shows the integrator control effort.

The spikes in the plant trajectory error are due to overshoot; they always occur near a sharp turn in the trajectory (see inset in Figure 9-a).